Supporting Information for

Revealing surface restraint induced hexagonal Pd nanocrystals via *in situ* transmission electron microscopy

Ruiyang You[1, §], Zhemin Wu[1, §], Jian Yu[1], Fei Wang[1], Shiyuan Chen[1], Zhong-kang Han[2], Wentao Yuan[1, *], Hangsheng Yang[1], and Yong Wang[1]

[1]Center of Electron Microscopy and State Key Laboratory of Silicon Materials, School of Materials Science and Engineering, Zhejiang University, Hangzhou, 310027, China.

[2] Fritz-Haber-Institut der Max-Planck-Gesellschaft, Faradayweg 4-6, 14195 Berlin, Germany.

[*]Corresponding author. Email: wentao_yuan@zju.edu.cn (W.Y.)

Table of Contents

Materials and methods:

1. **Preparation of icosahedral Pd nanocrystals (five-fold twinned Pd):**

   Icosahedral Pd nanocrystals covered with {111} facets were synthesized by a slightly modified chemical method developed by Xia et al.[1] In a typical synthesis, 2 mL of ethylene glycol (EG) and 20 mg of polyvinyl pyrrolidone (PVP) were mixed in a 25 mL single-necked flask and preheated to 160 °C under magnetic stirring. After 10 min, 1 mL EG solution containing 8.9 mg of Na_2PdCl_4 and 16.7 μL of HCl was injected into the flask. After that, additional 55 μL of HCl was added to the flask quickly. The reaction continued for further 10 min and instantly terminated by an ice-water bath. The collected products were washed by deionized water and acetone, and then dispersed in deionized water for further use.

2. ***In situ*** **TEM observation methods:**

   In this work, two type of heating chips were used to implement our *in situ* experiments. The most frequently used chip was that with amorphous carbon coating (E-AHBC, Protochips Aduro Heating), which was loaded on a heating holder and controlled by the facilities provided by Protochips company (Protochips Aduro 300 TEM). For the control experiments, heating chip with an amorphous SiN_x substrate was used, which was then loaded and controlled by the facilities provided by DENSsolutions company (Wildfire D6, DENSsolutions company). All the *in situ* TEM experiments were implemented in a FEI Cs-corrected transmission electron microscope (Titan G^2 80-300) operating at 300 kV. The dose rate was ~5×10^4 A/m^2s and the TEM column pressure was maintained at ~1×10^{-5} Pa during the experiments. The atomic resolution high angle annular dark-field (HAADF) images and EDX data were acquired by a Cs-corrected scanning transmission electron microscope (Titan G^2 80-200, ChemiSTEM, FEI) at room temperature, operated at 200 kV. The STEM column pressure was ~1×10^{-5} Pa, the convergence angle of HAADF was ~21.4 mrad, and the annular detection angle was set to be ~53-200 mrad. The heating rate in this work was 5 °C/s.

3. (S)TEM image simulations of Pd with different crystal phases:

The simulations of HAADF-STEM and TEM images were implemented by using the QSTEM software through multislice algorithm. Simulated electron diffraction images were performed by SingleCrystal (CrystalMaker SOFTWARE). The parameters for the simulations were set based on our experimental conditions.

4. DFT calculations:

First-principles calculations were carried out using density functional theory (DFT) with generalized gradient approximation (GGA) of Perdew-Burke-Ernzerhof (PBE) implemented in the Vienna Ab-Initio Simulation Package (VASP).[8, 9] The valence electronic states were expanded on the basis of plane waves with the core-valence interaction represented using the projector augmented plane wave (PAW) approach[10] and a cutoff of 400 eV. To investigate the function of graphene on fcc and hexagonal (hex) Pd, periodic slabs with (8 × 8) fcc and hex Pd unit cells were considered to model the (111) and (003) surface respectively, which both contains 4 layers. To simplify matters, the hex Pd model consists of only one Type II unit cell and 63 Type I unit cells, and corresponding three Pd atoms were removed to avoid steric crash (one Pd_{III} atom and two Pd_{II} atoms). Besides, the (9 × 9) unit cells of graphene with one layer was also built. Vacuum layers of 15 Å were added for all of three surfaces. After relaxation, the atoms of graphene surface were added to the fcc Pd and hex Pd surfaces, respectively. The initial distances between graphene and Pd surface were both large than 2 Å. A Γ-centered k-mesh of 1 × 1 × 1 was used due to the very large supercell size. Convergence is achieved when the forces acting on ions become smaller than 0.05 eV/Å.

Since fcc model has three atoms more than hex model, the total energy of fcc model was first averaged over atoms and then multiplied the atom number of hex model. For graphene involved fcc and hex models, the total energies should be deducted the energy of graphene, which based on the calculation of individual graphene model. Set the energy of fcc models as benchmarks, the relative energy of hex models can thus be derived.

Supporting Text:

1. Polymorphism of Pd NCs:

According to our best knowledge, the reported crystal phases of Pd contain fcc, hcp, hex, 4H and fct.[2-7] Since fct Pd NCs were only obtained by compress fcc Pd NCs with a huge pressure (~ 25 GPa) in a diamond-anvil cell, we excluded this structure in our work. As for the left Pd phases, the difference between them can be attributed to the stacking sequence of the close-packed planes. Fcc phase is accepted that adopts a repeated 'ABC' stacking, while hcp and 4H phase adopts a repeated 'AB' and 'ABAC' stacking, respectively.[2] For hex phase, it was proposed that one intact close-packed plane would be followed by two equivalent defective ones, which can be regarded as a 'ABB' stacking.[4]

Supporting Movie:

Movie S1. The in-situ observation of the fcc Pd icosahedron dispersed into small Pd NCs with different crystal phases from a top view. The dose rate was ~5×10^4 A/m^2s. The images in Figure 2a-d were collected from this movie. The movie plays with 128× normal speed.

Supporting Figures:

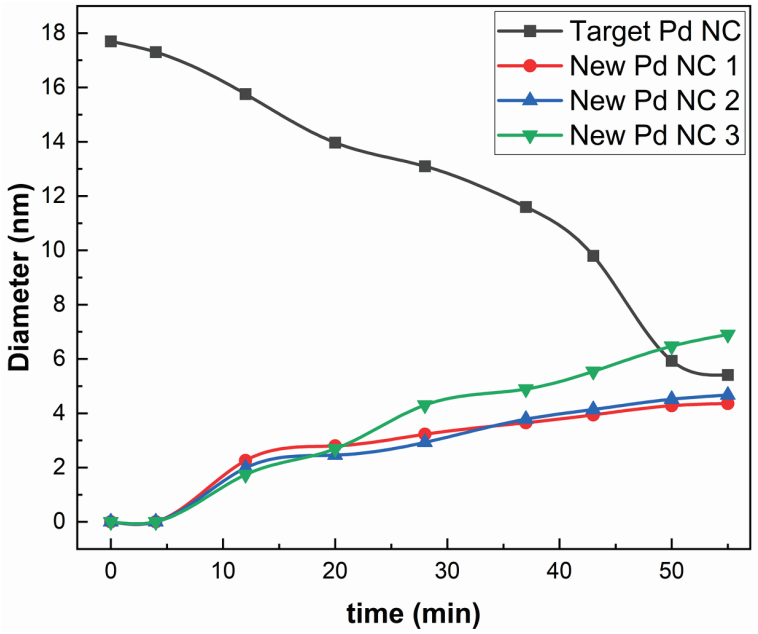

Figure S1. Diameter changes of the target Pd NC (denoted by red dotted circles in Figure 2e-h) and three new Pd NCs randomly selected.

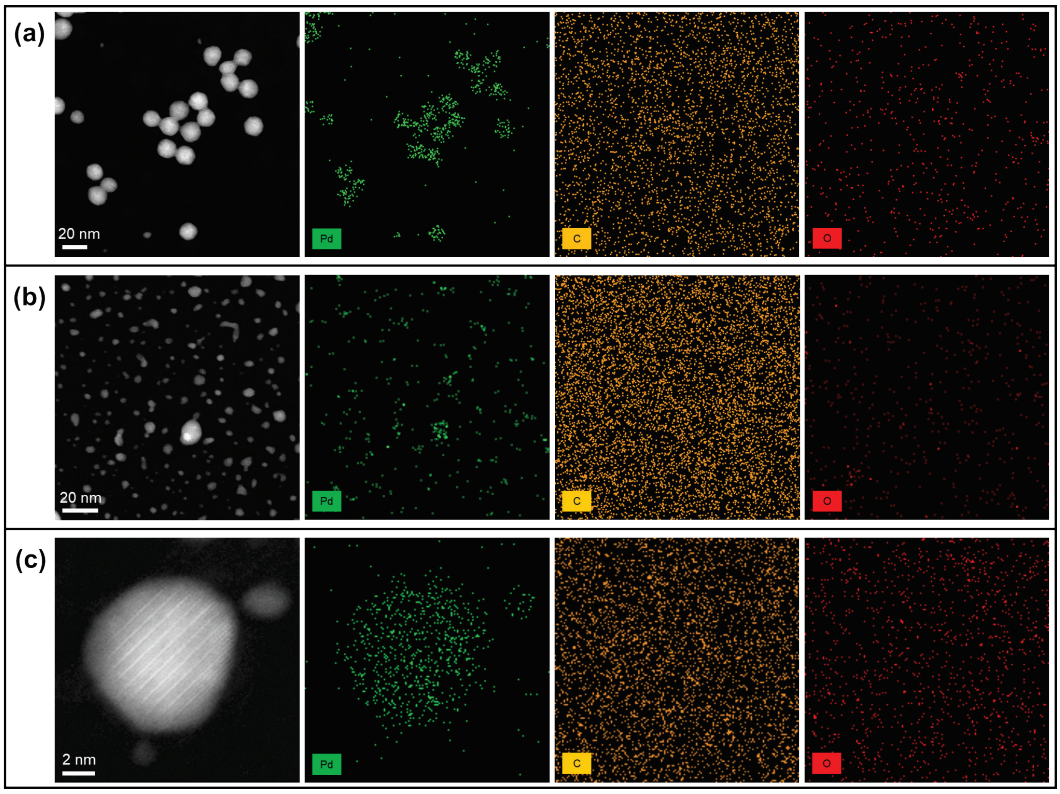

Figure S2. EDX elemental mappings of Pd nanocrystals before and after annealing (pressure: ~10^{-5} Pa; temperature: 20 °C). (a) As-prepared Pd icosahedrons before annealing. **(b)** New-formed Pd nanocrystals after annealing. **(c)** An individual hex Pd nanocrystal.

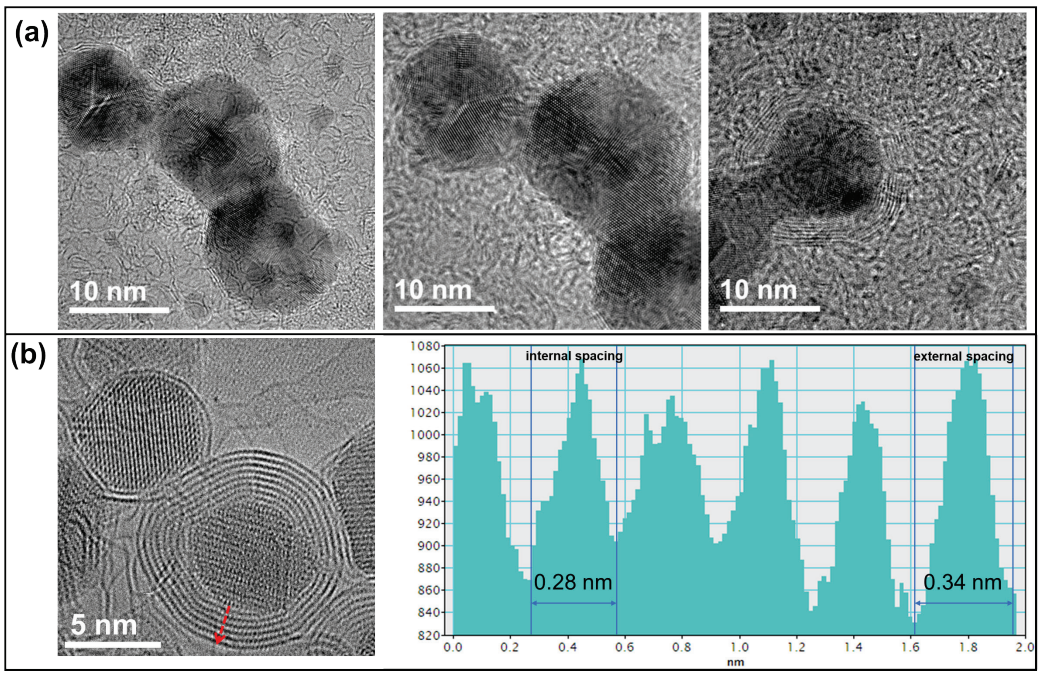

Figure S3. Compressed carbon onion. (a) TEM images of carbon onion (graphitic shells) encapsulated Pd icosahedrons. **(b)** Compressed carbon onion (left) and corresponding profile image (right).

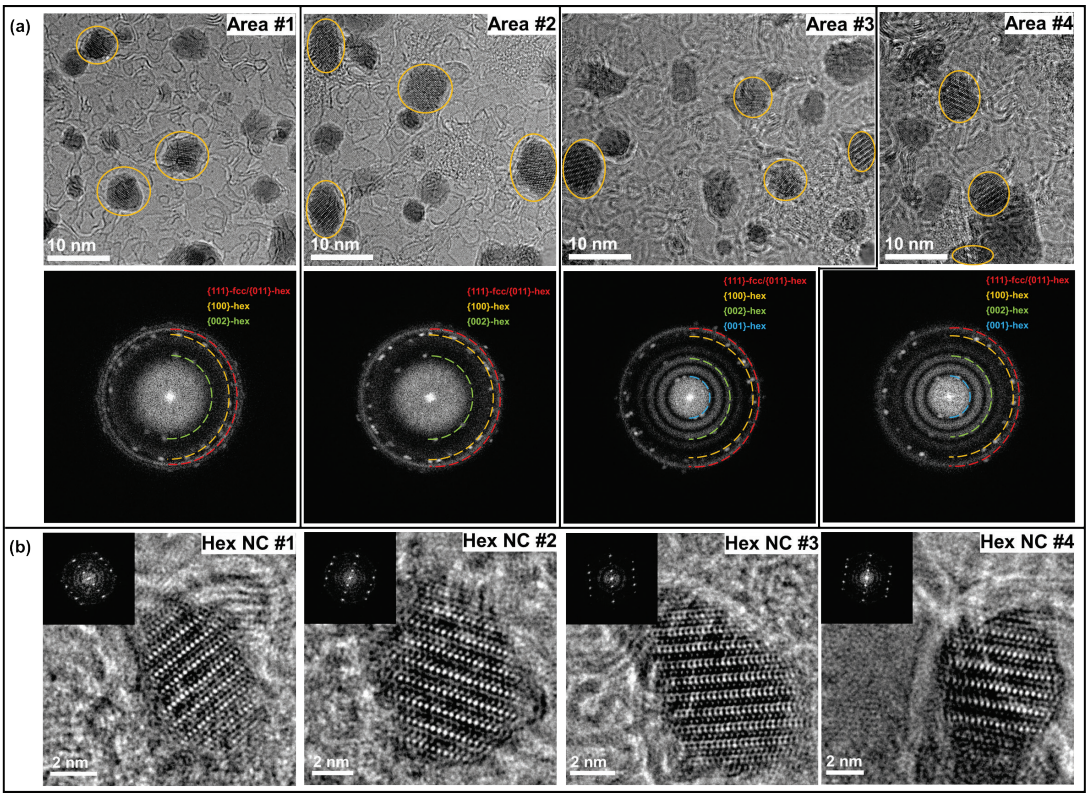

Figure S4. New phase (hex phase) of Pd NCs found in the dispersion process. (a) TEM images and corresponding FFT patterns of the new formed Pd NCs. The orange solid circles denote the hex Pd NCs. **(b)** HRTEM images of hex Pd NCs. Insets: single crystal FFT patterns.

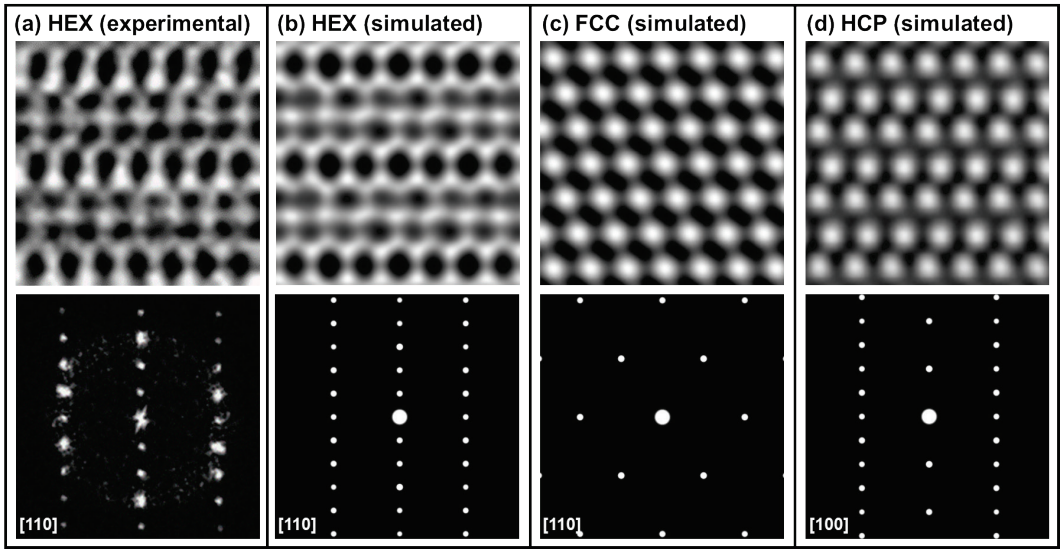

Figure S5. Comparison between hex, fcc, and hcp phases of Pd via HRTEM images. (a) Experimental HRTEM image of hex phase viewed along [110] direction and corresponding FFT pattern. **(b)** Simulated HRTEM image of hex phase viewed along [110] direction and corresponding FFT pattern. **(c)** Simulated HRTEM image of fcc phase viewed along [110] direction and corresponding FFT pattern. **(d)** Simulated HRTEM image of hcp phase viewed along [100] direction and corresponding FFT pattern.

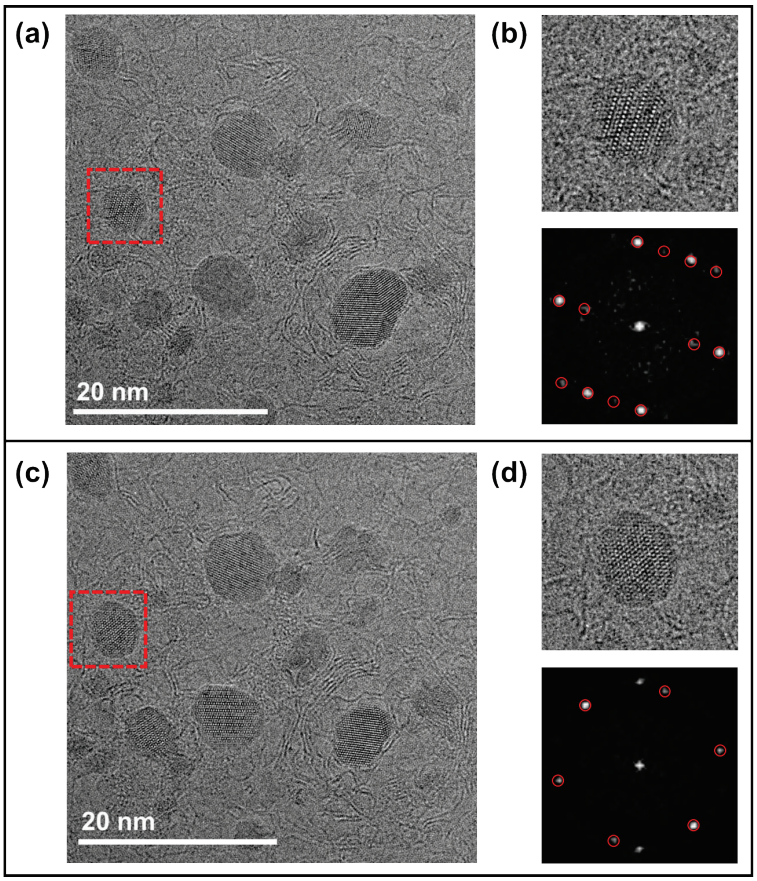

Figure S6. TEM images of the Pd viewed along two different directions. (a, c) TEM images collected from Movie S1 showing a hex Pd changed its orientation. **(b, d)** Enlarged TEM images and corresponding FFT pattern taken from the selected area in (a, c), respectively.

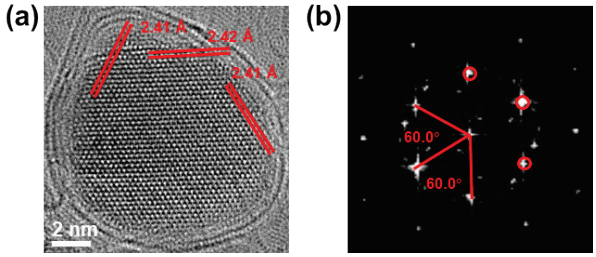

Figure S7. A HRTEM image of the hex Pd viewed along another typical direction (same as that in Figure S6d).

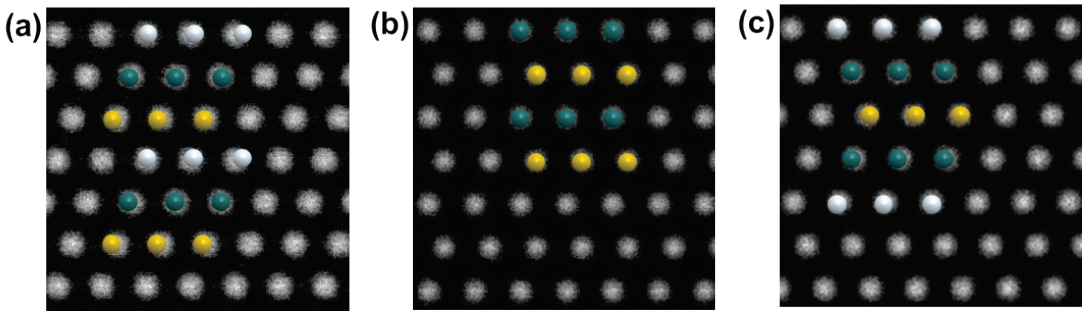

Figure S8. Simulated HAADF-STEM images of Pd. (a) Fcc phase, **(b)** Hcp phase and **(c)** 4H phase.

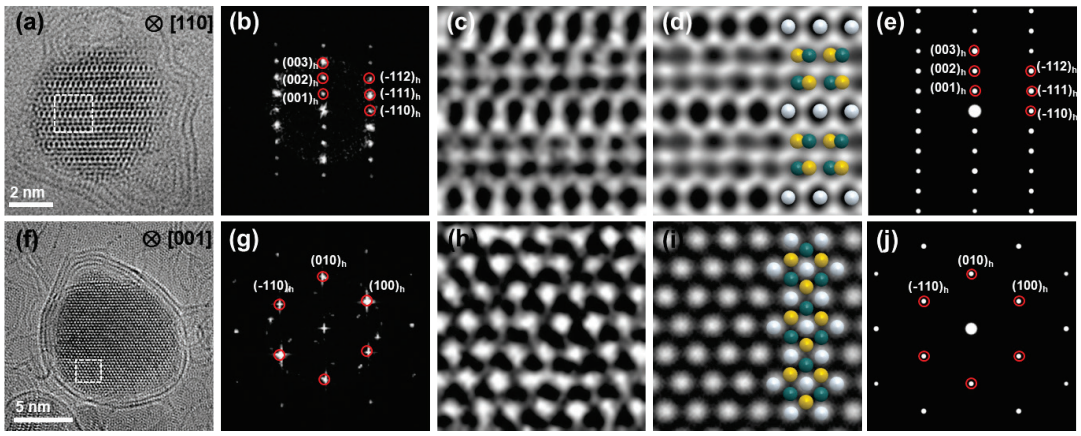

Figure S9. Experimental and simulated HRTEM images of hex Pd NCs viewing along two typical directions. (a, f) TEM images of hex Pd NCs viewed along [110] and [001] directions, respectively. **(b, g)** Corresponding FFT pattern taken from (a, e). **(c, h)** Enlarged images taken from the selected areas in (a, f). **(d, i)** Simulated TEM images viewed along [110] and [001] directions based on the hex Pd model. **(e, j)** Simulated electron diffraction pattern based on the (d, i).

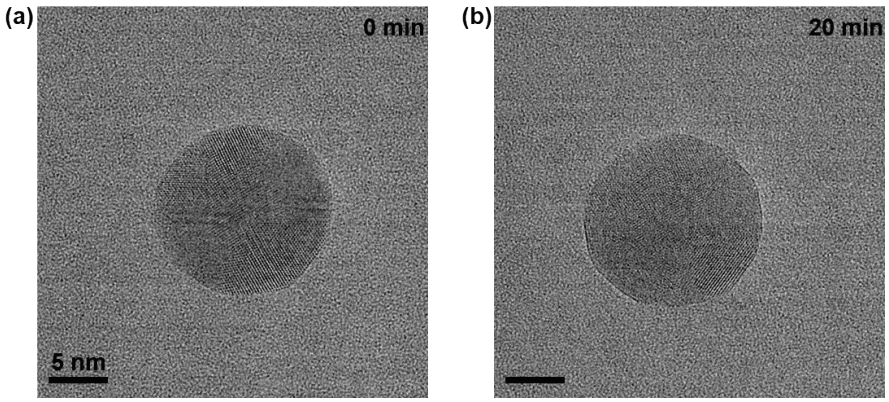

Figure S10. The control experiments performed on SiN_x support. (a, b) No dispersion process and hexagonal Pd nanocrystals were observed without carbon source. The images were acquired at 500 °C in vacuum (~10^{-5} Pa).

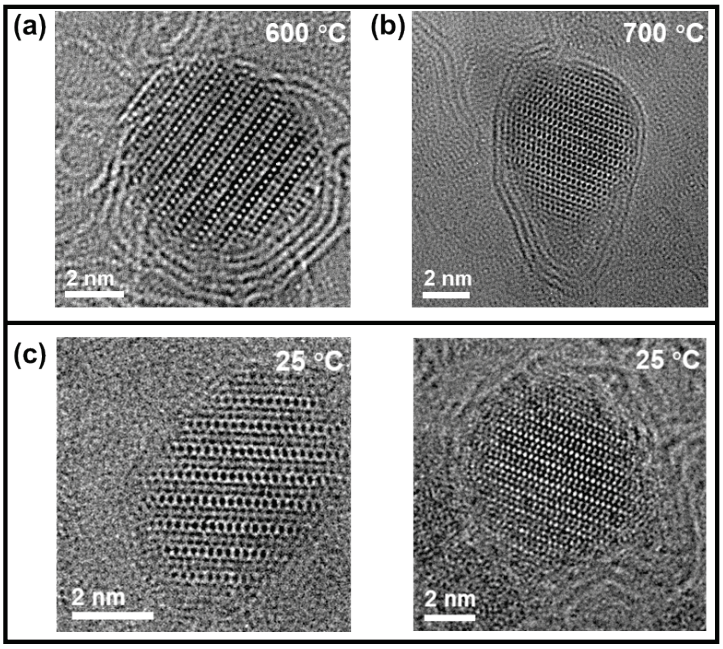

Figure S11. HRTEM images of the hex Pd NCs captured at different temperatures.

Supporting References:

1. Lv, T.; Wang, Y.; Choi, S.; Chi, M.; Tao, J.; Pan, L.; Huang, C.; Zhu, Y.; Xia, Y. Controlled Synthesis of Nanosized Palladium Icosahedra and Their Catalytic Activity towards Formic-Acid Oxidation. *ChemSusChem* **2013,** *6* (10), 1923-1930.
2. Janssen, A.; Nguyen, Q. N.; Xia, Y. Colloidal Metal Nanocrystals with Metastable Crystal Structures. *Angew. Chem., Int. Ed.* **2021,** *60* (22), 12192-12203.
3. Walter, J. Template-Assisted Growth of Hexagonal Poly- Or Single-Crystalline Quasi-2D Palladium Nanoparticles. *Adv. Mater.* **2000,** *12* (1), 31-33.
4. Meyer, H.; Mullerbuschbaum, H. New Form of Palladium Stabilized by Traces of Oxides. *J. Less-Common Met.* **1980,** *76* (1-2), 293-298.
5. Gao, K.; Wei, X.; Liu, G.; Zhang, B.; Zhang, J. Electrodeposition and Biocompatibility of Palladium and Phosphorus Doped Amorphous Hydrogenated Carbon Films. *Chem. Phys.* **2020,** *537*, 110857.
6. Chen, Y.; Fan, Z.; Luo, Z.; Liu, X.; Lai, Z.; Li, B.; Zong, Y.; Gu, L.; Zhang, H. High-Yield Synthesis of Crystal-Phase-Heterostructured 4H/fcc Au@Pd Core-Shell Nanorods for Electrocatalytic Ethanol Oxidation. *Adv. Mater.* **2017,** *29* (36), 1701331.
7. Guo, Q.; Zhao, Y.; Mao, W.; Wang, Z.; Xiong, Y.; Xia, Y., Cubic to Tetragonal Phase Transformation in Cold-Compressed Pd Nanocubes. *Nano Lett.* **2008,** *8* (3), 972-975.
8. Kresse, G.; Furthmüller, J. Efficient Iterative Schemes for ab Initio Total-Energy Calculations Using a Plane-Wave Basis Set. *Phys. Rev. B* **1996,** *54* (16), 11169-11186.
9. Perdew, J.; Burke, K.; Ernzerhof, M. Generalized Gradient Approximation Made Simple. *Phys. Rev. Lett.* **1998**, *77*(18), 3865-3868.
10. Blöchl, P. Projector Augmented-Wave Method. *Phys. Rev. B* **1994**, *50*(24), 17953-17979.